



Propagation rates of nonpremixed edge flames

Min Suk Cha^{a,*}, Paul D. Ronney^b

^a Environmental System Research Center, Korea Institute of Machinery & Materials, Daejeon, 305-343, Republic of Korea

^b Department of Aerospace and Mechanical Engineering, University of Southern California, Los Angeles, CA 90089-1453, USA

Received 7 August 2005; received in revised form 20 January 2006; accepted 22 February 2006

Available online 17 April 2006

Abstract

The propagation rates (U_{edge}) of nonpremixed ignition (advancing) fronts and extinction (retreating) edge flames were measured as a function of global strain rate (σ), jet spacing (d), mixture strength, stoichiometric mixture fraction (Z_{st}), and Lewis number (Le) using a counterflow slot-jet burner in which edge flames propagated along its long dimension. Electrical heaters at both ends of the slot “anchored” the flames, allowing conditions resulting in negative values of U_{edge} to be studied by triggering local extinction of anchored flames with an N_2 jet. Results are presented in terms of the effects of a dimensionless flame thickness (ε) related to σ and a dimensionless heat loss (κ) on a scaled U_{edge} . Propagation rates were markedly enhanced/retarded in mixtures with low/high Le . Propagation rates and extinction conditions were highly asymmetric with respect to $Z_{\text{st}} = 0.5$ despite the symmetry of flame location; mixtures with Z_{st} greater/less than 0.5 behaved like stronger/weaker mixtures, apparently due to the relative locations of the radical production zone and maximum temperature zone for varying Z_{st} . Two extinction limits were identified, corresponding to a high- σ strain-induced limit that was strongly dependent on Le but nearly independent of κ and a low- σ heat-loss-induced limit that was strongly dependent on κ but not Le . Most experimental findings were in good agreement with theoretical predictions; however, unlike predictions, “tailless” triple flames were not observed; instead standard triple flames and “short length” edge flames were found, and only for a very narrow range of experimental conditions. This is proposed to be due to the difference between the volumetric heat loss presumed in the models and the conductive transfer to the jet exits that dominates heat loss in the experiments.

© 2006 The Combustion Institute. Published by Elsevier Inc. All rights reserved.

Keywords: Nonpremixed edge flame; Advancing edge; Retreating edge; Short-length flame; Triple flame

1. Introduction

Recently “edge flames” have become a popular means to describe the behavior of premixed and nonpremixed flames where a transition from a burning to a nonburning state occurs along the length of the

flame sheet [1]. The nonburning state may exist ahead of an advancing (ignition) front or where the local conditions (strain rate, turbulence level, heat losses, etc.) are less favorable for combustion. Edge-flame models may be useful for understanding many types of non-uniform flame phenomena, e.g., flames stabilized near a cold wall or splitter plate, the leading edge of a flame spreading across a condensed-phase fuel surface, or flames in highly turbulent flow fields where “holes” in the flame sheet may open or “heal.”

* Corresponding author. Fax: +82 42 868 7284.

E-mail address: mscha@kimm.re.kr (M.S. Cha).

Theoretical studies of edge flames in both premixed [2–4] and nonpremixed [5–8] configurations predict that such edge flames propagate in a direction generally parallel to the flame sheet and exhibit a continuous spectrum of propagation speeds (U_{edge}) that may be positive (advancing into the unburned region), negative (retreating into the burned region), or zero depending on the environment, e.g., global strain rate (σ) or scalar dissipation rate, heat losses, Lewis number (Le), etc. According to these models, for moderate σ , $U_{\text{edge}} > 0$, whereas for sufficiently high values of σ , $U_{\text{edge}} < 0$. The condition $U_{\text{edge}} \rightarrow -\infty$ occurs as σ approaches that of the extinction strain rate (σ_{ext}) of the uniform (edgeless) flame. Between σ_{ext} and the (smaller) value of σ for which $U_{\text{edge}} = 0$, a continuous flame sheet could exist indefinitely, but should a hole develop locally in this sheet, for example, due to a locally high strain rate in a turbulent flow or the insertion of a heat sink, the resulting edge flame will have a negative propagation rate, resulting in growth of the hole and potentially complete extinction of the flame. Additionally, if heat losses are present, a second extinction limit may exist at sufficiently small σ . For nonpremixed flames, Daou et al. [7] expressed the combined effects of stain and heat losses in terms of a dimensionless flame thickness $\varepsilon \equiv \beta(\sigma\alpha/(2S_L^2))^{1/2}$, where β is the nondimensional activation energy (Zeldovich number), α the gas thermal diffusivity, and S_L the laminar burning velocity of a stoichiometric mixture of the fuel and oxidizer streams, and a dimensionless heat loss $\kappa \equiv \beta(\alpha/S_L^2)\kappa_0$, where κ_0 is a linear volumetric heat-loss coefficient (units s^{-1}). (ε can be interpreted as the square root of a scaled Karlovitz number, i.e., the ratio of strain rate to chemical rate, and κ the inverse square of a Peclet number based on S_L .)

The aforementioned theoretical studies assumed constant gas density in order to suppress the effects of hydrodynamics, in particular the thermal expansion of the gases due to heat release, and thereby focus on diffusive-thermal effects. However, U_{edge} is in fact strongly influenced by thermal expansion. By considering the effect of thermal expansion on the momentum of the gases, Ruetsch et al. [9] showed that for adiabatic nonpremixed edge flames, in the limit of sufficiently small scalar dissipation rate, U_{edge} scales with $S_L(\rho_u/\rho_b)^{1/2}$, where ρ_u is the unburned gas density and ρ_b is the gas density in the combustion products. The predicted ratio of U_{edge} to $S_L(\rho_u/\rho_b)^{1/2}$ is close to unity but not quite constant. We shall incorporate this scaling into the interpretation of our experimental results.

While a large number of theoretical and computational studies of edge flames have been conducted, experimental studies are considerably fewer in num-

ber. In particular, no studies have confirmed or refuted the predicted effect of σ on U_{edge} over an extended range of σ . Additionally, no experimental studies have systematically addressed the effects of environmental parameters such as mixture strength, stoichiometric mixture fraction (Z_{st}) (which affects the flame position relative to the stagnation plane; many experiments have employed fuel–air mixtures that have very small Z_{st} and thus the flame resides far on the air side of the stagnation plane), Lewis number, and impact of heat loss. It is to be noted that Z_{st} is defined as $Z_{\text{st}} = 1/(1 + \nu X_f/X_o)$, where ν is the stoichiometric oxygen to fuel mass ratio, X_f and X_o represent the initial mass fraction of fuel and oxygen for each stream, respectively. Probably the most comprehensive study to date is that of Ko et al. [10], who studied the effect of fuel concentration gradient (varying from fully premixed to fully nonpremixed) on U_{edge} in methane–air mixtures but did not study any of the aforementioned parameters nor the high- σ or low- σ near-limit behavior.

In addition to the lack of a comprehensive database of U_{edge} , there is still controversy as to whether negative edge-flame speeds can be observed experimentally. In a study of vortices interacting with nonpremixed flames, Amantini et al. [11] found no evidence to suggest that negative edge speeds existed for any value of σ . In contrast, Carnell and Renfro [12], using a coannular counterflow burner to create a strain-rate gradient that extinguished the perimeter of a central nonpremixed flame, reported stable edge flames with $U_{\text{edge}} < 0$ in this configuration. However, in the experiments by Amantini et al. the hydrodynamic environment in which the flame exists is both temporally and spatially varying, and in Carnell and Renfro it is spatially varying. Moreover, in both cases there is a velocity gradient in the direction of edge-flame propagation as well as orthogonal to it, which make comparisons of these experiments to model predictions more difficult, since the aforementioned models assume a plane strain in the plane orthogonal to the direction of propagation of the edge flame or a mixture fraction gradient only in the direction orthogonal to the plane of the flame sheet. Additionally, the method of obtaining negative edge speed employed by Carnell and Renfro requires a velocity difference between the inner and the outer jets; to avoid shear-layer instabilities the approach is limited to very low jet velocities and thus very low σ (13 s^{-1} in their case).

Numerous flow configurations have been used to study strained uniform flames and edge flames. Perhaps the most common is the axisymmetric counterflowing jet apparatus. A difficulty with this apparatus in the context of the current study is that extensional strain occurs in both coordinate directions parallel to

the flame surface. In contrast, a counterflow *slot-jet* apparatus provides extensional strain in the direction orthogonal to the plane of the slots but there is very little strain or convection in the direction along the length of the slots. Thus, the flame is strained only in one of the two coordinates in the plane of the flame. In this way, an edge flame that is nearly unstrained in the direction of propagation can be obtained. Additionally, computations by Ashurst et al. [13] have shown that highly strained regions of turbulent flows exhibit a most probable ratio of strain along the three principal axes in the ratio 0.75:0.25:–1, where positive values denote extensional strain. Moreover, DNS studies of premixed flames [14] have shown that the flame surface normal preferentially aligns with the most compressive strain direction, and that the strain in the plane of the flame is statistically much higher in one direction than the orthogonal direction in the plane of the flame. Thus, highly strained regions, where strain effects are most important, do not typically exhibit nearly equal rates of extensional strain in the plane of the flame along two of the principal axes. The counterflow slot-jet configuration provides strain rates in the ratio 1:0:–1 whereas round jets provide 0.5:0.5:–1. Thus, the slot-jet configuration provides straining characteristics that are more representative of the conditions of flames in strongly turbulent flows than axisymmetric jets provide. Additionally, because the convection velocity in the long dimension of the slot is very small, the propagation speed in the laboratory frame is nearly equal to the propagation speed relative to the cold unburned gas far ahead of the edge flame (or behind, in the case of retreating edge flames). This simplifies the interpretation of the experimental data.

Consequently, the goal of the present investigation is to study the effects of strain rates (by varying jet-exit velocity and burner separation distance), mixture strength (by varying the level of dilution with an inert gas), impact of heat loss (by varying jet spacing), Lewis number (by varying fuel and diluent type), and flame location relative to the stagnation surface (by varying stoichiometric mixture fraction) on the propagation rates of nonpremixed edge flames in a counterflow slot-jet configuration and thereby provide a detailed map of their dynamics and extinction properties. Investigation of premixed edge flames is deferred to a subsequent paper. The experimental results are compared with theoretical predictions for both ignition fronts and extinction fronts of nonpremixed edge flames [6,7]. Also, the effects of gas expansion on maximum propagation speeds of edge flames will be discussed and compared to the numerical predictions for two-dimensional mixing layers [9].

2. Experiment design

To exploit fully the advantages of slot-jet counterflows for studying edge flames, some consideration of the operability limits of this configuration is needed. Four such limits have been identified. The first two are limits intended for study, namely the high- σ strain-induced limit and the low- σ heat-loss-induced limit discussed in the Introduction. The third and fourth limits are hydrodynamic limits, namely turbulence and buoyancy, that should be avoided. Consequently, the goal of the experiment design is to identify conditions for which the first and second limits can be studied without interference from the third and fourth limits. Below are the estimated criteria for these limits.

- *Strain-induced extinction:* Daou et al. [7] predict that for $Le \approx 1$, $\varepsilon \approx 2.5$ at this limit, and that this limit is nearly independent of the heat-loss parameter κ . Because equal jet velocities are employed and the densities of the two streams are nearly equal, $\sigma = 2U_{jet}/d$. Thus, the extinction criterion is $U_{jet} \approx (2.5/\beta)^2(S_L^2 d/\alpha)$.
- *Heat-loss-induced extinction:* Daou et al. [7] predict that the heat-loss limit occurs at $\varepsilon \approx 15\kappa$. κ_0 is a volumetric heat-loss coefficient which can be estimated as $hA\Delta T/(\rho C_p V \Delta T)$, where the heat transfer coefficient $h \approx 3.77k/d$ for laminar flow between two infinite parallel plates, k is the gas thermal conductivity, A is the area for heat transfer (twice the area of 1 jet exit cross section, A_{jet}), and V is the gas volume ($A_{jet}d$). Hence, $\kappa_0 \approx 3.77(k/d)(A)/(\rho C_p A_{jet}d) \approx 7.54\alpha/d^2$, thus $\kappa \approx \beta(\alpha/S_L^2)(7.54\alpha/d^2) \approx 7.54\beta(\alpha/(S_L d)^2)$, and finally the criterion for extinction is $U_{jet} \approx (15)^2(7.54)^2(\alpha/d)^3/S_L^2$. (Note that with a suitably defined flame Peclet number $Pe_{flame} \equiv S_L d/\alpha$, $\kappa = 7.54\beta/Pe_{flame}^2$; for premixed flames Pe_{flame} and thus κ is nearly constant at the limit because the characteristic flame thickness and thus the volume suffering heat losses are proportional to α/S_L which is nearly independent of σ , whereas for nonpremixed flames Pe_{flame} and κ at the limit depend substantially on σ because the mixing layer thickness scales with $(\alpha/\sigma)^{1/2}$.)
- *Turbulent flow:* A transition to unsteady and probably turbulent flow was observed in preliminary experiments at $Re_{jet} \equiv U_{jet}w/\nu > 500$, where w is the jet width ($= 0.5$ cm for our experiments) and ν the gas viscosity at ambient conditions. This transition was nearly independent of the jet spacing d .
- *Buoyancy-dominated flow:* At sufficiently low U_{jet} , unstable, gravity wave-like flame behav-

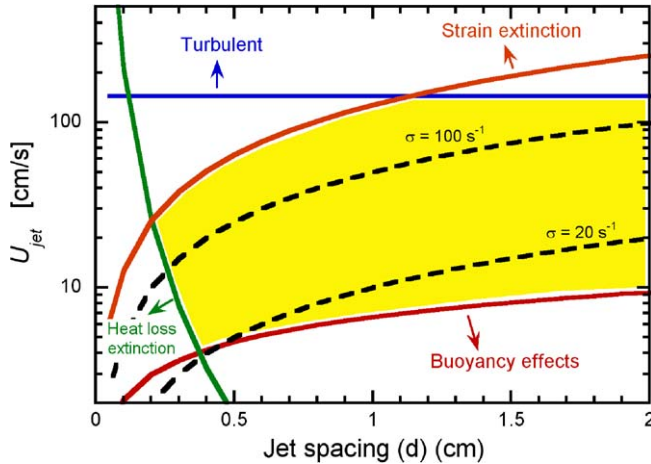


Fig. 1. Operating conditions for slot-jet burning for the “baseline” mixture (see Table 1). The shaded region denotes the desired range of operating parameters.

ior was observed, apparently due to buoyancy-induced convection. An estimate (that was found to be consistent with experimental observations) of the condition for which buoyancy effects become significant is when U_{jet} equals the buoyant convection velocity $\approx 0.3\{g(d/2)\}^{1/2}$, where $d/2$ rather than d is chosen as the characteristic dimension because (when $Z_{\text{st}} = 0.5$, thus the flame is centered with respect to the jets) only the upper half of the jet gap contains gas with an unstable density gradient. (An independent estimate based on the mixing layer thickness rather than $d/2$ for our experimental parameters coincidentally yields nearly the same result.)

These four estimated limit criteria are plotted in Fig. 1 for the baseline mixture. For these calculations α is evaluated at ambient temperature; a temperature-averaged value could potentially provide more accurate estimates, but the increase in α with temperature will be offset to a large extent by an increase in convection velocity due to thermal expansion; thus properties such as mixing layer thickness may not be strongly affected by the temperature change. The operable parameter space of the experiment is the shaded region between the limits. Also shown for reference are the combinations of U_{jet} and d providing two values of the strain rate σ in the range of interest. Fig. 1 shows that smaller values of d are preferable to study the heat-loss limits but at too small d no flames can be established, and at large d turbulence prevents study of the strain extinction limit. Since it is desirable to cover the entire range of σ (thus U_{jet}) between the heat-loss and the strain extinction limits minimal effects of turbulence or buoyancy, we chose $d = 0.75$ cm as the baseline condition.

3. Experimental apparatus

The counterflow slot-jet burner employed for the experiments consisted of two 0.5×13 -cm central rectangular jets. The upper jet contained a mixture of oxidizer (O_2) and inert (N_2 or CO_2) and the lower jet contained a mixture of fuel (CH_4 or C_3H_8) with the same inert as the upper jet. Equal values of U_{jet} were employed for the upper and lower streams. On both sides of these jets, additional 0.5×13 -cm slot jets provided N_2 sheath flow to prevent the formation of a secondary nonpremixed flame with ambient air. The interior of all six jets was filled with steel wool and the jet exits were fitted with stainless-steel honeycomb of 0.7-mm channel width to ensure uniformity of the exit flow. The jets (and thus the gases at the jet exits) were maintained at room temperature by water cooling. Commercial mass-flow controllers with accuracy $\pm 1\%$ of full scale (calibrated with wet-test meters) controlled the gas flows. The sheath flow velocities (U_{sheath}) were matched to those of the central jets, i.e., $U_{\text{sheath}} = U_{\text{jet}}$, to avoid shear-layer instabilities between the reactive flow and sheath flows. This choice also produced flames that were nearly flat and parallel to the jet exit planes. Fig. 2 shows that U_{edge} is fairly insensitive to U_{sheath} for a range of velocities near this choice. The entire apparatus was enclosed in a ventilated box to minimize potential interference from room drafts at low U_{jet} .

Propagating edge flames ($U_{\text{edge}} > 0$) were easily produced by establishing a uniform flame in the counterflow, extinguishing or “erasing” the flame starting from one end of the jet and moving to the other end by sweeping a small (3-mm-diameter) round jet of N_2 across the length of the slot, leaving only a small burning region at one end, and then suddenly removing the N_2 jet. This procedure resulted in an edge flame

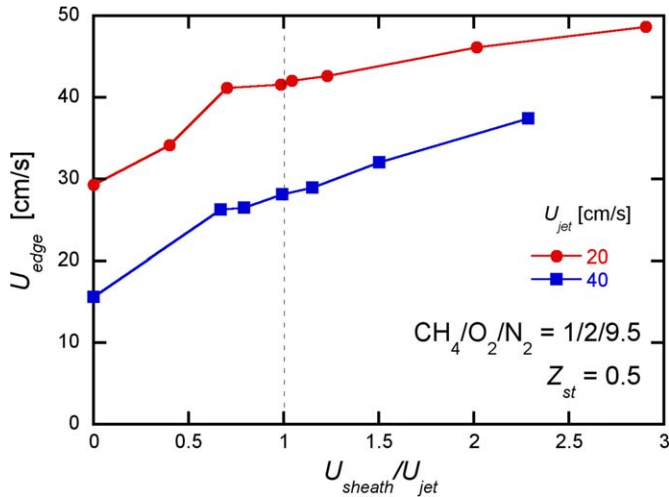


Fig. 2. Effect of sheath flow velocity on edge-flame propagation velocity (U_{edge}) for the “baseline” mixture (see Table 1).

that propagated across the length of the slot, thereby reestablishing the uniform flame. Producing retreating edge flames ($U_{edge} < 0$) is much more problematic. One cannot merely establish a flame in the counterflow and trigger extinction at one end because in the counterflow slot-jet apparatus there is little or no convection velocity in the direction of propagation/retreat of the edge flame, and thus the condition at the flame end is $U_{edge} = 0$. This condition occurs for the stretch/heat-loss limits at lower/higher σ than the value of σ at extinction of the uniform (edgeless) flame (σ_{ext}). Consequently, the range of conditions for which $U_{edge} < 0$ is not directly accessible in a slot-jet apparatus with “bare” slot ends. To overcome this limitation, electrical wire resistance heaters attached to ceramic spacers (Fig. 3) were installed at both ends of the slots. The wire temperature was about 1300 K. These heaters substantially increased the total mixture enthalpy near the ends of the slot, thereby creating locally a mixture with $U_{edge} > 0$ that “anchored” the weaker unheated mixture away from the ends of the slot. Retreating edge flames could then be triggered with a jet of N_2 that both extinguished the flame in an unheated region adjacent to the end heaters and prevented the heaters from reigniting the flame end.

Propagation of the edge flames was recorded by a color digital video camera (framing rate 30 Hz, shutter speed 10 ms) with a wide-angle lens viewing the entire length of the slot jets. The flame edge location as a function of time was determined by frame-by-frame analysis of these video records.

Close-up flame images were recorded using an intensified CCD camera with 2-ms shutter speed. For the fastest propagating case (~ 60 cm/s), the flame edge travels about 1.2 mm during the exposure time,

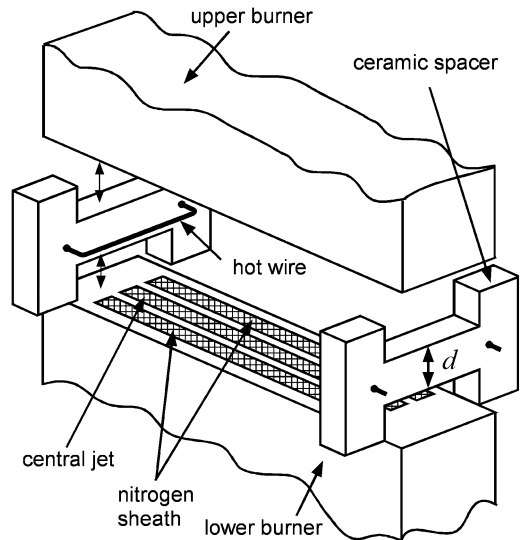


Fig. 3. Schematic of ceramic burner spacer with electrically heated wire.

which corresponds to 22 pixels for the ICCD camera. In this regard, we can say that the images are well resolved. We used a 105-mm focal length UV lens with an aperture of f4.5 and the distance between the lens and the center of burner was 30 cm. From this information, we can estimate that the depth of field is about 2 mm. The flame thickness difference within this 2-mm depth of field will be less than 1%; thus we believe that misinterpretation due to the setup of collecting optics is negligible.

Table 1 shows the conditions tested in this work. Values of S_L shown in this table were computed for stoichiometric premixtures of the fuel and oxidizer streams using the Sandia flame code with the GRI 3.0

Table 1

Experimental conditions and corresponding flame properties (“baseline” conditions are shown in bold)

Mixture composition (volume ratio)	Inert ratio (Q)	S_L (cm/s)	d (cm)	Z_{st}	$(\rho_u/\rho_b)^{1/2}$	α (cm ² /s)	β	κ
CH ₄ /O ₂ /N ₂ (1/2/ Q) ($Le_{fuel} = 0.96$; $Le_{O_2} = 1.10$)	6.00	57.9	0.75	0.5	2.84	0.201	9.58	0.0015
	9.00	25.5	0.75	0.5	2.64	0.201	10.8	0.0090
			0.5,					0.0270,
			0.75,	0.5				0.0120,
			1.0					0.0067
			0.75	0.2,				0.0120
				0.8				
	10.0	19.2	0.75	0.5	2.57	0.200	11.2	0.0163
	11.0	14.1	0.75	0.5	2.51	0.200	11.6	0.0312
	11.75	11.0	0.75	0.5	2.47	0.200	11.9	0.0526
12.0	10.1	0.75	0.5	2.46	0.200	12.0	0.0630	
12.25	9.28	0.75	0.5	2.44	0.200	12.2	0.0757	
12.5	8.50	0.75	0.5	2.43	0.200	12.3	0.0908	
CH ₄ /O ₂ /CO ₂ (1/2/ Q) ($Le_{fuel} = 0.74$; $Le_{O_2} = 0.86$)	4.09	25.2	0.50	0.5	2.77	0.133	14.0	0.0118
	4.35	21.9	0.50	0.5	2.74	0.131	14.2	0.0153
	4.85	16.7	0.50	0.5	2.69	0.129	14.6	0.0264
	5.28	13.0	0.50	0.5	2.64	0.127	14.9	0.0431
	6.50	6.07	0.50	0.5	2.53	0.123	16.0	0.1980
	7.10	4.17	0.50	0.5	2.48	0.121	16.5	0.4198
C ₃ H ₈ /O ₂ /N ₂ (1/5/ Q) ($Le_{fuel} = 1.86$; $Le_{O_2} = 1.05$)	16.6	56.0	0.68	0.5	2.89	0.182	9.08	0.0016
	20.0	39.9	0.68	0.5	2.78	0.185	9.61	0.0034
	23.0	28.7	0.68	0.5	2.70	0.186	10.0	0.0069
	26.2	20.5	0.68	0.5	2.61	0.187	10.5	0.0143
	27.6	17.7	0.68	0.5	2.58	0.188	10.8	0.0198
	28.9	15.0	0.68	0.5	2.54	0.188	11.0	0.0281

chemical kinetics mechanism [15] and Wang mechanism [16] for methane and propane fuel, respectively. The Zeldovich number β is given by $E(T_f - T_\infty)/(RT_f^2)$, where T_f is the adiabatic flame temperature, T_∞ the ambient temperature, and E/R the activation temperature which was calculated from a linear fit of $\ln(S_L)$ vs $1/T_f$, the slope of which is $-E/2R$. κ was estimated as described in the previous section.

For each set of the parameters d , mixture strength, stoichiometric mixture fraction Z_{st} , fuel type, and inert type as listed in Table 1, edge-flame propagation speeds were measured for the entire range of σ from the low- σ heat-loss limit to the high- σ strain extinction limit. The baseline mixture was chosen to be (on a mole basis) 15.1% CH₄/84.9% N₂ on the fuel side and 33.9% O₂/66.1% N₂ on the oxidizer side, for which $Z_{st} = 0.5$ and thus the flame location corresponds to the stagnation plane. CH₄/N₂ against O₂/N₂ was chosen because the Lewis numbers of both CH₄ and O₂ are near unity and $Z_{st} = 0.5$ was chosen since most theoretical works employ this condition. When combined in stoichiometric proportions, the resulting mixture is CH₄/O₂/N₂ = 1/2/9.5; to facilitate comparisons, mixtures will be specified in terms of this stoichiometric fuel/O₂/N₂ mole ra-

tio along with Z_{st} . For the baseline case, $d = 0.75$ cm was chosen for the reasons discussed in the previous section. To assess heat-loss effects, baseline mixtures with $d = 0.5$ and 1.0 cm were tested. To assess the effects of Z_{st} , the baseline mixture was retained but a portion of the N₂ diluent was moved to either the CH₄ or the O₂ stream such that $Z_{st} = 0.2/0.8$. Then, again we matched jet velocities for each stream with newly calculated concentrations of CH₄ and O₂, which correspond to (34.5% CH₄, 20.8% O₂) and (9.7% CH₄, 91.5% O₂) for $Z_{st} = 0.2$ and 0.8, respectively. In this way, the flame location moves toward the O₂ or CH₄ side of the stagnation plane. Finally, CH₄/O₂/CO₂ and C₃H₈/O₂/N₂ mixtures were tested to investigate the effects of low and high Lewis numbers, respectively. Slightly different values of the jet spacing d were employed for these cases so that d/α is constant, i.e., to maintain the same flame Peclet number for the same S_L .

Results are reported in terms of the *global* strain rate $\sigma = 2U_{jet}/d$. While the *local* strain rate will vary in the streamwise direction due to thermal expansion effects, for the present purposes the global strain rate is considered to be the more appropriate parameter, especially considering that correlations of strain effects for turbulent flames [17] employ global

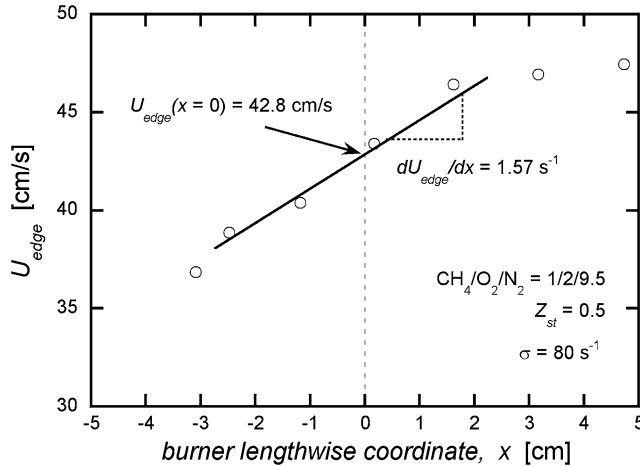


Fig. 4. Example of effect of edge-flame location on propagation rate in the laboratory reference frame.

strain rate estimates based on the cold-gas conditions. Moreover, far ahead of the flame front, in the cold-gas, constant-density region, the simple relation $\sigma = 2U_{\text{jet}}/d$ is valid. Furthermore, most theoretical works on edge flames employ the constant-density assumption, thereby sidestepping the issue of flow-field modification near the flame edge due to thermal expansion [4,6–8]. Indeed, it is unclear whether a unique “local” strain rate can be defined for a two-dimensional structure such as an edge flame, considering how difficult it has been to determine a proper definition of strain rate at the flame front for a conventional one-dimensional counterflow flame and how to extrapolate these data to zero strain rate to determine the unstretched laminar burning velocity [18].

While a slot aspect ratio of 26:1 was employed to create a nearly plane strain in the plane orthogonal to the edge-flame propagation direction with little flow in the propagation direction, and the ceramic spacers/heaters (Fig. 3) at the ends of the slot-jets minimize this flow still further, for proper determination of U_{edge} it is still necessary to account for this flow. To accomplish this, the edge-flame propagation speed in the laboratory frame of reference (as determined from the video records) was plotted as a function of position (x) along the slot. A nearly linear relationship between $U_{\text{edge}}(x)$ and x was found, an example of which is shown in Fig. 4. This strongly suggests that the edge-flame velocity *relative to the unburned gas* is essentially constant and that there is a small, nearly constant velocity gradient along the slot of magnitude $dU_{\text{edge}}(x)/dx$. Consequently, a linear least-square fit was applied to the data in the vicinity of the center of the slot and interpolated to determine U_{edge} at the burner center where symmetry requires that there is no flow in the propagation direction and thus values of U_{edge} in the laboratory frame and relative to the gas

are identical. This value of U_{edge} is reported in the results below. Note that for the example shown in Fig. 4, $dU_{\text{edge}}(x)/dx$ is 51 times smaller than the primary strain rate σ ; for all conditions examined this ratio was greater than 25 (i.e., comparable to or greater than the slot aspect ratio). Therefore, the velocity gradient in the direction of edge-flame propagation does not influence the results significantly.

4. Results

4.1. Effect of jet spacing

Fig. 5 shows the effect of strain rate σ on edge-flame propagation rate U_{edge} in terms of the nondimensional flame thickness ε as a function of the scaled propagation rate $U_{\text{edge}}/(S_L(\rho_u/\rho_b)^{1/2})$ for jet spacings (d) of 0.5, 0.75, and 1.0 cm. For a large range of ε , the scaled edge-flame speed is positive and has a nearly constant value of about 0.8. At sufficiently large or small ε , the propagation rate decreases and becomes negative for a relatively small range of ε close to the extinction limits. The decrease is more precipitous at low ε ; consequently, it was very difficult to obtain small but still positive propagation speeds near the small- ε extinction limit. The high- ε condition for which $U_{\text{edge}} = 0$ corresponds to the stationary edge flames in small strain rate gradients studied previously [19]. Except for the low- ε region, the propagation and extinction characteristics for all three d are very similar, with extinction occurring at $\varepsilon \approx 2.1$. This similarity suggests that the global strain rate $\sigma = 2U_{\text{jet}}/d$ is indeed an appropriate measure of strain rate. The difference at low ε is likely due to heat losses; since $\kappa \approx 7.54\beta(\alpha/(S_L d))^2$, as d decreases, the heat-loss parameter κ increases (see Table 1) and

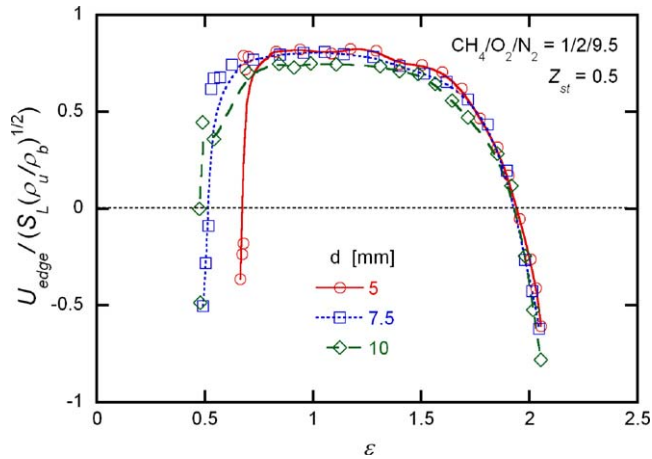


Fig. 5. Effect of nondimensional flame thickness ε on scaled U_{edge} for $Z_{\text{st}} = 0.5$, $\text{CH}_4/\text{O}_2/\text{N}_2 = 1/2/9.5$, and various d .

thus the range of ε over which flames can be sustained is smaller.

Fig. 6 shows images of the visible flame emissions, false-colored for easier visualization. For the baseline mixture, the flame is nearly centered between the jets since $Z_{\text{st}} = 0.5$. As ε increases, the mixing layer thickness and thus the visible flame thickness decrease. For retreating flames at high ε , the edges are more tapered (less blunt) than advancing edges are, as predicted by Daou et al. [7]. However, unlike Daou et al.'s predictions, no triple flame structures were observed for the baseline mixture even at very low ε . This observation will be discussed further in the next section.

4.2. Effect of mixture strength

Fig. 7a shows the effect of dimensional strain rate σ on the unscaled edge-flame propagation rate U_{edge} for several dilution levels and thus different κ . As the N_2 dilution level and thus κ increases, U_{edge} decreases for all values of σ and the range of σ over which flames can be sustained decreases. For $\text{CH}_4/\text{O}_2/\text{N}_2$ mixtures weaker than about 1/2/11.75, only negative edge speeds can be obtained, and beyond 1/2/12.5, no flames could be obtained for any σ . The high- σ extinction strain rate for $\text{CH}_4/\text{O}_2/\text{N}_2 = 1/2/11$ of about 90 s^{-1} is close to the value of 100 s^{-1} reported by Kitajima et al. [20] for round jets. An interesting feature of Fig. 7a is that the maximum value of U_{edge} occurs at $\sigma \approx 30 \text{ s}^{-1}$ (shown as a dashed vertical line in Fig. 7a) for all dilution levels. For the stronger mixtures, i.e., lower dilution levels, U_{edge} is nearly constant for a wide range of σ straddling 30 s^{-1} , whereas for the weaker mixtures U_{edge} peaks distinctly near $\sigma = 30 \text{ s}^{-1}$. For *adiabatic* flames, the maximum value of U_{edge} occurs at $\sigma = 0$ [7], but with

heat loss the maximum U_{edge} will occur at a larger σ for which heat losses are less significant, but σ is not so large that the strain effects start to reduce U_{edge} . An estimate of the minimum σ for which heat losses are insignificant is when the ratio of jet spacing d to mixing layer thickness $\sim (\alpha/\sigma)^{1/2}$ is sufficiently large. This ratio can be expressed as $\text{Pe}_{\text{jet}}^{1/2}$, where $\text{Pe}_{\text{jet}} \equiv U_{\text{jet}}d/\alpha$ is the Peclet number based on U_{jet} and d . For $\sigma = 30 \text{ s}^{-1}$ and $d = 0.75 \text{ cm}$, $\text{Pe}_{\text{jet}} = 42$. The data in Fig. 7a indicate that this criterion for the maximum value of U_{edge} is independent of the mixture strength and thus is independent of S_L and κ . In other words, regardless of the ratio of conductive heat loss to the jet exits to heat generation by the flame (characterized by κ), the optimal condition for edge-flame propagation is set by the smallest value of σ where this heat loss is insignificant (characterized by Pe_{jet}).

Fig. 7b shows the same data as in Fig. 7a but scaled as in Fig. 5. Fig. 7b shows that the scaling of strain rate by ε as in Daou et al. [7] and propagation speed by $U_{\text{edge}}/S_L(\rho_u/\rho_b)^{1/2}$ as in Ruetsch et al. [9] provides an appropriate means to compare data sets at varying dilution levels. Note that at intermediate $\varepsilon \approx 1.5$ all mixtures except very weak ones have nearly the same scaled propagation speed. For larger $\varepsilon \approx 2$ edge-flame speeds become negative for all mixtures, and complete extinction ($U_{\text{edge}} \rightarrow -\infty$) occurs at $\varepsilon = 2.3 \pm 0.3$. In contrast, the low- ε behavior is very different for different mixtures; stronger mixtures having smaller κ can survive at much smaller ε .

The behavior seen in Figs. 5 and 7b is very similar to that predicted by Daou et al. [7] in that (1) the peak propagation speed occurs for intermediate ε , with a relatively smooth drop at large ε and a more precipitous drop at small ε , (2) the maximum scaled edge-flame speed is slightly less than unity (though Daou

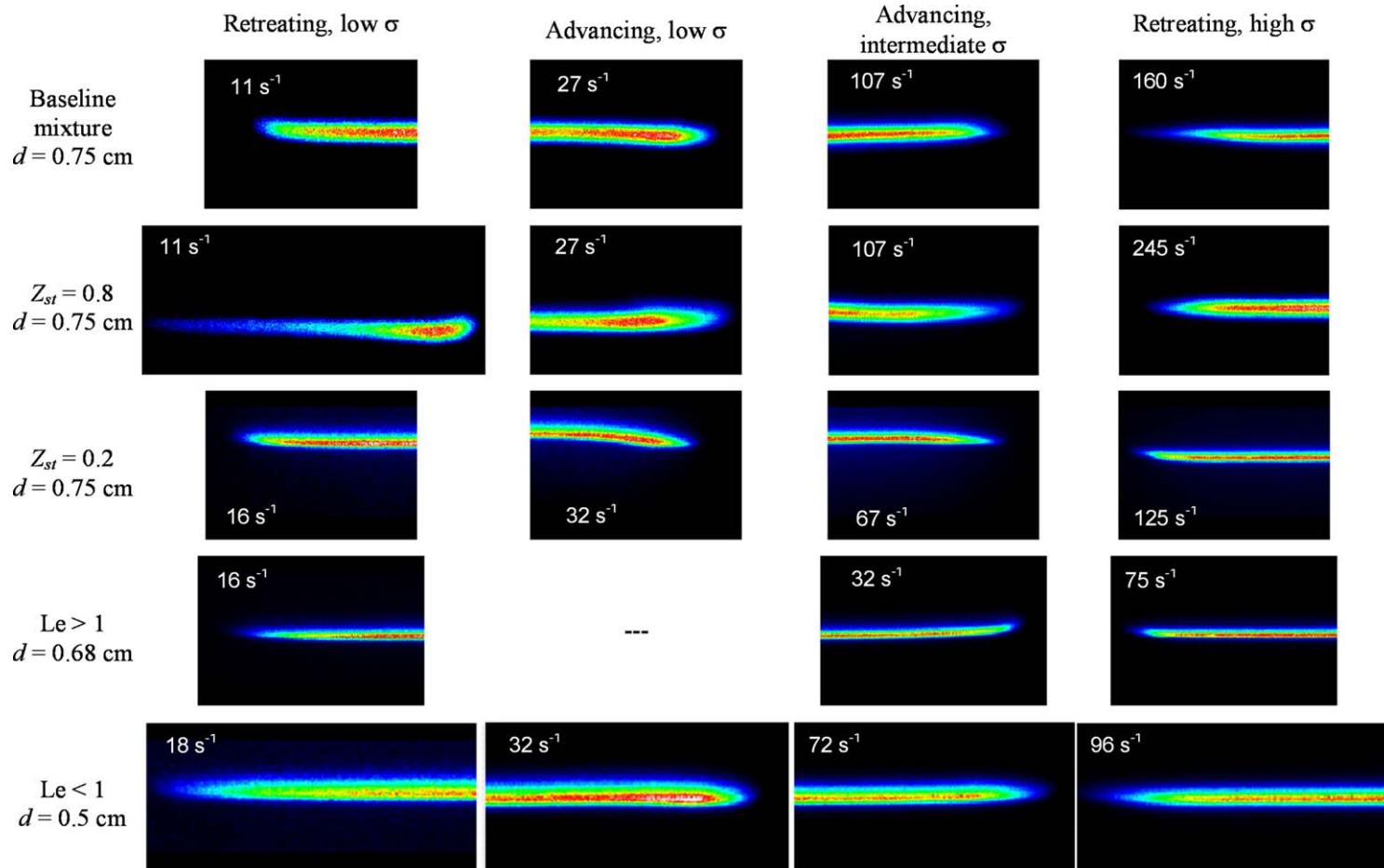


Fig. 6. False-color images of direct emission from edge flames. The global strain rate (σ) is shown in upper left-hand corner of each image. The fuel/oxygen enters from the bottom/top of these images. All flames propagate from left to right. The height of each image corresponds to the jet spacing.

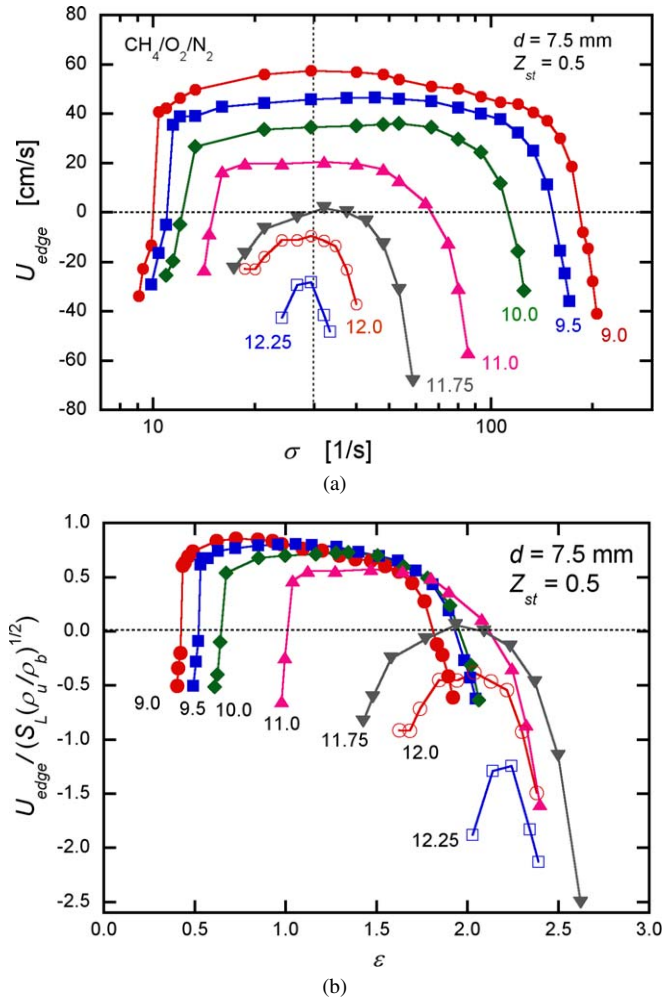


Fig. 7. Effect of dimensional strain rate (σ) on dimensional U_{edge} for $d = 7.5$ mm, $Z_{st} = 0.5$, and various N₂ dilution ratios in CH₄/O₂/N₂ mixtures. Number (Q) associated with each curve refers to the dilution level in terms of CH₄/O₂/N₂ = 1/2/ Q . (a) Raw data. (b) Scaled U_{edge} vs nondimensional flame thickness ϵ .

et al. only considered $\rho_u/\rho_b = 1$, so the effect of density change from Ruetsch et al. [9] is employed), and (3) for κ greater than about 0.05 (corresponding to CH₄/O₂/N₂ = 1/2/11.75, see Table 1) there is no positive edge speed for any value of ϵ .

On the other hand, there are differences between our results and Daou et al.'s [7] predictions at low ϵ . In particular, the experiments show that negative edge speeds exist for all mixtures at low ϵ , whereas Daou et al. predict this only for $\kappa > 0.04$. Daou et al. also found a separate disconnected branch of positive edge speed solutions at very low ϵ , even for $\kappa > 0.04$, but we could not find such behavior experimentally. Nevertheless, the discontinuous behavior predicted by Daou et al. is somewhat reminiscent of the precipitous change from positive to negative edge speeds at low ϵ seen experimentally. The most likely reason for the

discrepancies between model and experiment is that Daou et al. assumed a volumetric heat loss with no conductive heat sink, whereas experimentally the loss to the jet exits is gradient-driven. While modeling of gradient-driven losses as a volumetric term has been used to model extinction limits for a long time with surprisingly accurate predictions [21], in the context of the current study the mixing layer thickness can grow only to the point where it is comparable to d before the entire flame structure is disrupted, whereas with volumetric heat losses the mixing layer thickness can grow indefinitely as σ decreases. Consistent with this explanation, Daou et al. predict that the low- ϵ , positive edge-speed branch of solutions occurs only at $\epsilon < 0.5$, which corresponds to $\sigma = 10$ s⁻¹, $U_{jet} = 3.8$ cm/s, and thus $Pe_{jet} = 20$ for the baseline conditions, which is in the regime where the mixing

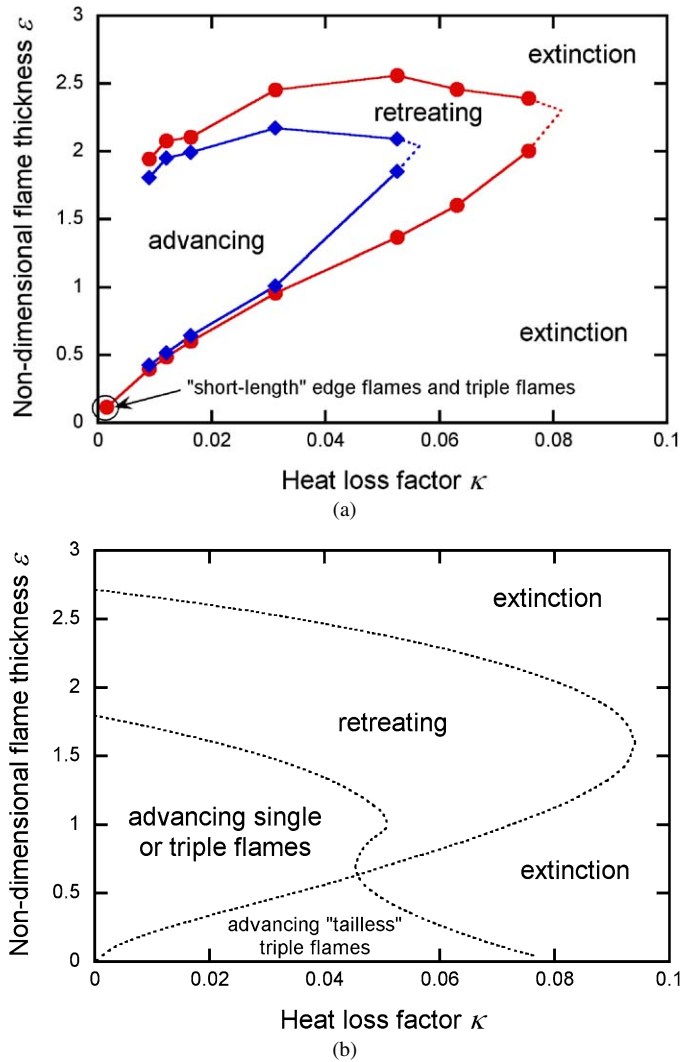


Fig. 8. Map of propagation modes and extinction limits of edge flames with heat-loss factor κ and nondimensional flame thickness ε . (a) Experimental results for $\text{CH}_4/\text{O}_2/\text{N}_2$ mixtures with $d = 0.75$ cm and $Z_{\text{st}} = 0.5$. (b) Theoretical predictions from Daou et al. [7].

layer thickness is comparable to d . (To study experimentally the case where volumetric losses due to radiation dominate conductive losses to the jet exits, much larger d would be required, which would in turn necessitate low-gravity conditions to avoid buoyancy-induced flow instabilities.) Moreover, this low- ε , positive edge-speed branch of solutions corresponds to conditions where *tailless triple flames* are predicted by Daou et al. whereas no such structures were observed experimentally. For tailless triple flames, the low σ and consequently large mixing layer thickness and volume enable the volumetric heat losses to extinguish the trailing diffusion-flame part of the triple-flame structure whereas the leading edge, which has a premixed flame-like structure with thickness pro-

portional to α/S_L (independent of σ), does not extinguish. With gradient-driven losses the impact of such losses on the premixed and nonpremixed parts of the triple-flame structure cannot be separated in this way; thus a tailless triple flame does not appear.

To summarize the effects of mixture strength in a compact form, a map of flame behavior in κ - ε space is shown in Fig. 8a along with the corresponding predictions by Daou et al. [7] in Fig. 8b. There are numerous similarities between the two plots: (1) the strain-induced extinction limit occurs near $\varepsilon = 2.5$ and is not strongly dependent on κ ; (2) the heat-loss-induced limit occurs along a limit line with roughly $\varepsilon \sim \kappa$; (3) the ultimate extinction limit, where the strain and heat loss limits converge, is near $\kappa = 0.08$.

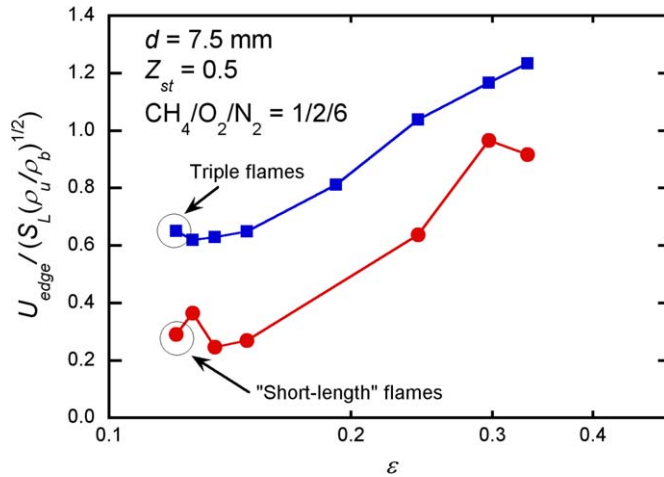


Fig. 9. Effect of nondimensional flame thickness ϵ on scaled U_{edge} for $\text{CH}_4/\text{O}_2/\text{N}_2 = 1/2/6$, $d = 7.5$ mm, and $Z_{st} = 0.5$.

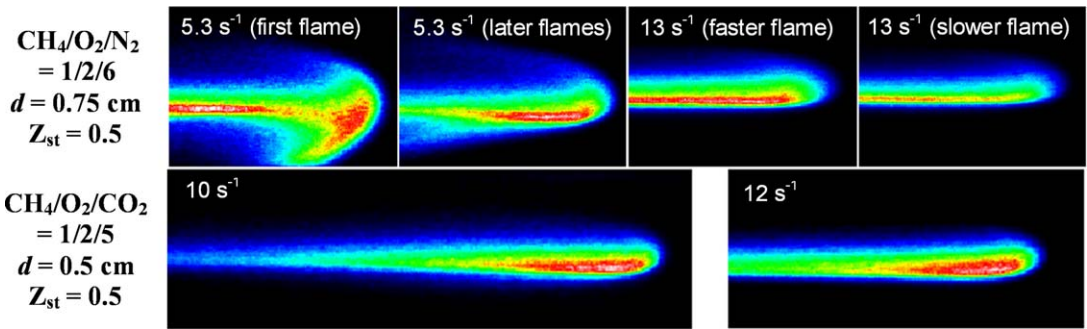


Fig. 10. Images of “short-length” and continuous (tail not extinguished) edge flames in very strong mixtures at low σ . Global strain rate (σ) is shown in upper left-hand corner of each image. The fuel/oxygen enters from the bottom/top of these images. All flames propagate from left to right. The height of each image corresponds to the jet spacing. For the $\text{CH}_4/\text{O}_2/\text{N}_2$ flames at $\sigma = 5.3 \text{ s}^{-1}$, the “first flame” is that propagating into a cold, unreacted flow whereas “later flames” is a typical image of one of many flames in a “train” of “short-length” flames. For the $\text{CH}_4/\text{O}_2/\text{N}_2$ flames at $\sigma = 13 \text{ s}^{-1}$, both images were taken with the same camera settings to compare the brightness of the “fast” and “slow” flames.

However, in the low- ϵ , moderate- κ regime predicted to exhibit tailless triple flames, experiments showed only extinction. In fact, triple flames (with or without tails) were not observed in any of the experiments described above; only single advancing or retreating edge flames were observed. As discussed above, the most likely reason for this discrepancy is the difference between the mechanisms of heat loss present in the experiments compared to that assumed in the theoretical model.

In an attempt to observe triple flames, a very strong mixture ($\text{CH}_4/\text{O}_2/\text{N}_2 = 1/2/6$) with correspondingly high S_L was studied at low σ in order to obtain very low ϵ where Daou et al. [7] and others have predicted that “standard” or “tailless” triple flames may exist. It should be noted that buoyancy effects are prevalent at such low σ (Fig. 1), so quantitative comparison with predictions may be imprac-

tical. Propagation speeds for these conditions are shown in Fig. 9. Two distinct propagation speeds were observed, but there was no means to prescribe which type of flame was obtained in a given experiment. Sometimes there was a transition from the slow flame to the fast flame during a test, but the reverse was not observed. Images of these flames are shown in Fig. 10. The faster flame is broader and brighter than the slower one, but even the broader flame does not exhibit distinct lean and rich premixed-flame branches characteristic of triple flames except very close to the low- ϵ extinction limit where distinct triple-flame structures were observed for the first edge flame propagating into a cold mixture. This leading triple-flame triggered the spontaneous formation of a continuous train of short-length edge flames that have a propagating leading edge and a retreating trailing edge. Under such conditions the heated wire at

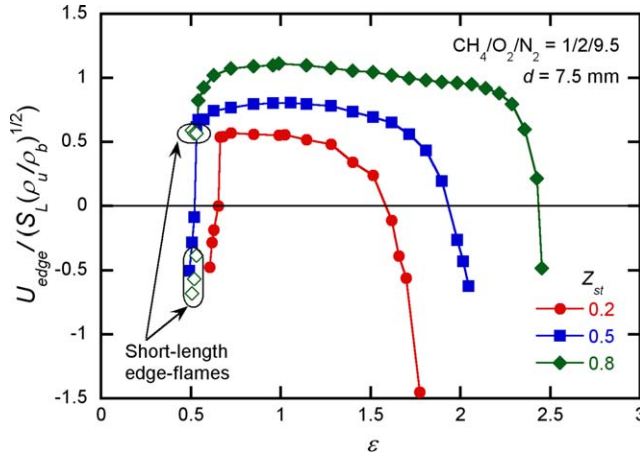


Fig. 11. Effect of nondimensional flame thickness ε on scaled U_{edge} for $\text{CH}_4/\text{O}_2/\text{N}_2 = 1/2/9.5$, $d = 7.5$ mm, and various Z_{st} . Each “short-length” edge flame for $Z_{\text{st}} = 0.8$ at very low ε has a propagating and a retreating edge, both of which are shown.

the end of the slot acts as a continuous source of short-length edge flames with a Strouhal number (ratio of shedding frequency to σ) of 0.3–0.4. As Fig. 9 shows, the triple-flame speed followed the trend of the faster flames at higher ε , whereas the short-length flame speed followed the trend of the slower flame. In some cases the magnitude of the trailing edge speed was different than that of the leading edge, in which case the length of the “short-length” flame was not constant. Apparently the short-length flames exist because the leading triple-flame leaves behind a combination of reactants and products that is too weak (due to reactant depletion and heat losses) to sustain a trailing diffusion flame, but once this mixture is swept out of the vicinity of the mixing layer on a time scale of the order $1/\sigma$, another edge flame initiated by the heated wire can propagate across the slot. By comparison, Ko et al. [10] did not observe triple flames in nonpremixed methane–air counterflow slot-jet experiments but did observe a transition from a single nonpremixed flame to a broader flame head and possibly a triple-flame structure as the mixture was changed from a purely nonpremixed flame to a partially premixed flame (i.e., some fuel added to the O_2 side and vice versa) which increased the mixing layer thickness.

4.3. Effect of stoichiometric mixture fraction

The effect of stoichiometric mixture fraction Z_{st} on edge-flame propagation speeds for the baseline $\text{CH}_4/\text{O}_2/\text{N}_2 = 1/2/9.5$ mixture and $d = 0.75$ cm is shown in Fig. 11. The same premixed S_L and T_f are assumed for all Z_{st} because the Lewis numbers of fuel and O_2 are both near unity in which case T_f is independent of Z_{st} and thus flame location. Fig. 11 shows that as Z_{st} increases, U_{edge} is higher for the same ε

and the low- ε and high- ε extinction limits are wider (though only slightly so for the low- ε limit). The images in Fig. 6 show that, as expected, the flames with low/high Z_{st} lie on the oxygen/fuel side of the stagnation plane and the leading edges curve toward the stagnation plane. As σ (thus ε) increases, this shift is less pronounced since the mixing layer thickness decreases. For a given σ , the low- Z_{st} flames are noticeably thinner. Also, short-length edge flames (but no triple flames) were observed at low ε for $Z_{\text{st}} = 0.8$ whereas for $Z_{\text{st}} = 0.5$ such flames were observed only for a much stronger mixture (see Fig. 9). Thus, edge flames are considerably stronger/weaker when the flame lies on the fuel/oxidizer side of the stagnation plane. Note that there are no differences in mechanical aspects, such as the flow field and heat loss, between $Z_{\text{st}} = 0.2$ and 0.8. One might therefore expect that edge-flame behavior should be symmetrical with respect to $Z_{\text{st}} = 0.5$ (where the flame is located at the midplane between the jet exits) and that if the flame location is moved closer to one jet exit due to an increase or decrease in Z_{st} , at low σ the flame would be weaker because of increased heat loss to the closer jet exit. The observed behavior is decidedly different. Analogous behavior has recently been reported for uniform (edgeless) nonpremixed flames by Kitajima et al. [20] and Chen and Axelbaum [22]. For a $\text{CH}_4/\text{O}_2/\text{N}_2 = 1/2/7.52$ mixture, for Z_{st} increasing from 0.2 to 0.8, Chen and Axelbaum reported an increase in σ_{ext} by a factor of about 1.9, which is practically the same as we observed for a 1/2/9.5 mixture (when inspecting Fig. 11 to glean such information, recall $\varepsilon \sim \sigma^{1/2}$). Chen and Axelbaum attribute this behavior to a shift in the O_2 concentration profile as Z_{st} increases to coincide more closely with the location of peak temperature, which in turn increases radical production rates and leads to a more robust

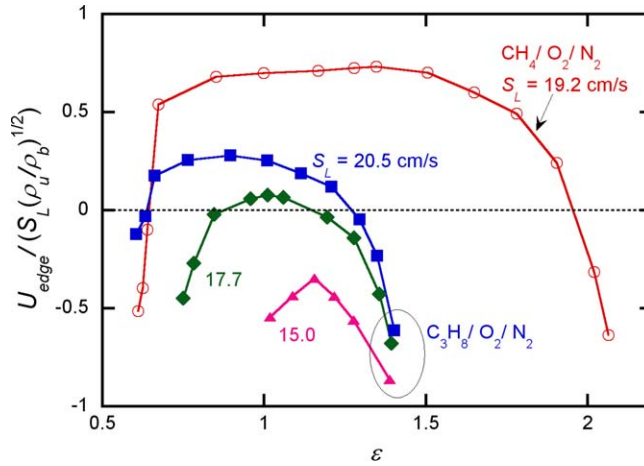


Fig. 12. Effect of nondimensional flame thickness on scaled U_{edge} with for $\text{C}_3\text{H}_8/\text{O}_2/\text{N}_2$ mixtures ($Le > 1$) with different N_2 dilution levels, $d = 6.8$ mm, and $Z_{\text{st}} = 0.5$. Also shown for comparison is a case for $Le \approx 1$ ($\text{CH}_4/\text{O}_2/\text{N}_2 = 1/2/10.0$, $d = 7.5$ mm, and $Z_{\text{st}} = 0.5$).

flame. It is to be noted that though we did not specifically test inverted flames with varying Z_{st} , Kitajima et al. [20] showed that there is no significant difference between the standard and inverted configurations for varying Z_{st} .

4.4. Effect of Lewis number

The effects of the nondimensional flame thickness ϵ on the scaled edge-flame propagation speed for fuel Le larger than unity are shown in Fig. 12. To compare with the $Le \approx 1$ case, data for $\text{CH}_4/\text{O}_2/\text{N}_2 = 1/2/10$ mixtures, which have the similar S_L as the strongest $\text{C}_3\text{H}_8/\text{O}_2/\text{N}_2$ mixture tested, are also shown. Fig. 12 shows that values of U_{edge} are much smaller for the $Le > 1$ case even at the similar S_L (thus nearly the same heat-loss parameter κ) and same ϵ . The high- ϵ extinction limit occurs at $\epsilon \approx 1.4$ for all $\text{C}_3\text{H}_8/\text{O}_2/\text{N}_2$ mixtures tested, which is much smaller than the $\epsilon \approx 2.3 \pm 0.3$ found for the $Le \approx 1$ mixtures. In contrast, for the similar κ the low- ϵ limits are practically the same for $Le \approx 1$ and $Le > 1$. For each $\text{C}_3\text{H}_8/\text{O}_2/\text{N}_2$ data set shown in Fig. 12, the maximum value of U_{edge} occurs at a dimensional strain rate slightly larger than the 30 s^{-1} value found for $\text{CH}_4/\text{O}_2/\text{N}_2$ mixtures (Fig. 7a) and thus nearly the same Pe_{jet} (note the slightly smaller d for the $\text{C}_3\text{H}_8/\text{O}_2/\text{N}_2$ data) which gives further support to the notion that this maximum is not related to any specific chemical or diffusive process but is merely the smallest value of σ where the effects of heat loss to the jet exits are insignificant. Consequently, the low- ϵ heat-loss-induced extinction limit is practically unaffected by Le . This is consistent with predictions by Daou et al. [8].

The images in Fig. 6 show that the high- Le flames are substantially thinner for the same σ and S_L than those with $Le \approx 1$ or $Le < 1$. Also, the flame lies on the fuel side of the stagnation plane since the fuel diffusivity is less than the oxygen diffusivity; thus a higher gradient is needed on the fuel side to obtain a stoichiometric ratio of mass fluxes. This behavior is again less pronounced at higher σ where the mixing layer thickness is smaller. The leading edge of the propagating flame curves upward, i.e., from the fuel side ($Le > 1$) toward the oxygen side ($Le \approx 1$) for moderate σ (thus ϵ), but this curvature disappears at high σ where $U_{\text{edge}} < 0$. These shapes are consistent with predictions by Daou and Liñán [6] for fuel $Le > 1$, oxygen $Le = 1$.

Edge-flame propagation speeds for $Le < 1$ mixtures are shown in Fig. 13. Because of the use of $\text{CH}_4/\text{O}_2/\text{CO}_2$ mixtures, in this case fuel and oxygen Lewis numbers are nearly equal and both are less than unity (see Table 1); thus the flame is very near the stagnation plane (see Fig. 6). Fig. 13 shows that $Le < 1$ mixtures have much higher values of scaled U_{edge} than $Le \approx 1$ mixtures having similar S_L (thus κ). Also, unlike the $Le \approx 1$ or $Le > 1$ mixtures, for $Le < 1$, U_{edge} continues to increase with increasing ϵ well past the point where heat losses have ceased to be significant. This is because moderate strain increases reaction rates only for $Le < 1$. Of course, sufficiently high strain still causes extinction, but for $Le < 1$ mixtures U_{edge} drops more precipitously as the high- ϵ extinction limit is approached than is the case for $Le \approx 1$ or $Le > 1$ mixtures. These observations are again consistent with theoretical predictions by Daou and Liñán [6]. The high- ϵ extinction limit occurs at $\epsilon = 5.6 \pm 0.9$ for the mixtures shown in Fig. 13, which is much higher than that for $Le \approx 1$

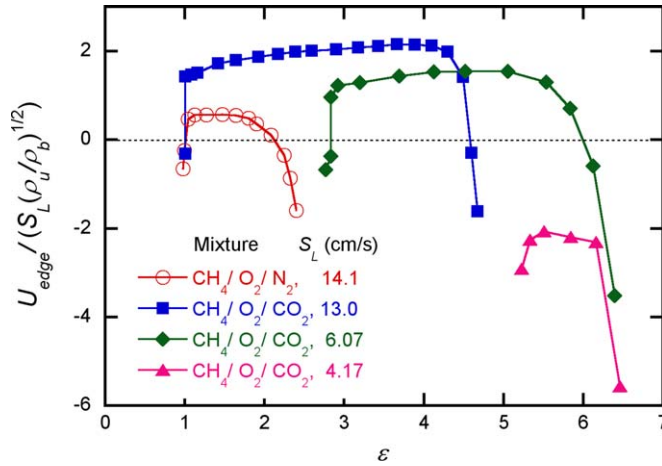


Fig. 13. Effect of nondimensional flame thickness on scaled U_{edge} with for $\text{CH}_4/\text{O}_2/\text{CO}_2$ mixtures ($Le < 1$) with different CO_2 dilution levels, $d = 5$ mm, and $Z_{st} = 0.5$. Also shown for comparison is a case for $Le \approx 1$ the baseline condition ($\text{CH}_4/\text{O}_2/\text{N}_2 = 1/2/11$, $d = 7.5$ mm, and $Z_{st} = 0.5$).

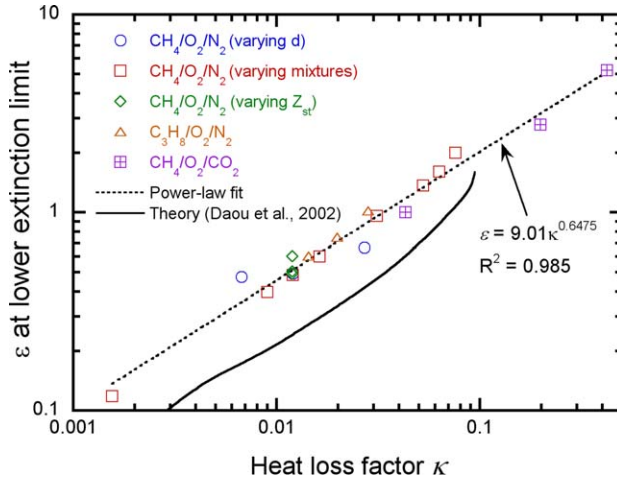


Fig. 14. Nondimensional flame thickness (ϵ) at low-strain (heat-loss-induced) extinction limit as a function of nondimensional heat loss (κ) for all conditions tested in this work, along with theoretical predictions by Daou et al. [7] for $Le = 1$.

mixtures (Fig. 7b) or $Le > 1$ (Fig. 12), but for each mixture family having nearly the same Le , the extinction limits are nearly independent of S_L (thus κ). In contrast, the low- ϵ heat-loss-induced extinction limit occurs at nearly the same ϵ for the $Le < 1$ and $Le \approx 1$ mixtures having nearly the same S_L (thus κ). This is further evidence that the low- ϵ heat-loss-induced extinction limit is practically unaffected by Le . To quantify this assertion further, Fig. 14 shows the correlation between ϵ at the low-strain extinction limit and the heat-loss parameter κ for all low- ϵ limits measured in this study. The data covering a nearly 3-decade range of κ fit a simple power-law relation with exponent 0.65 reasonably well with no noticeable influence of Le (though note that extinction data can be obtained at higher κ in low- Le mixtures be-

cause ϵ at the strain-induced limit is larger at lower L ; thus the convergence of the strain-induced extinction limit and the heat-loss-induced extinction limit is pushed out to higher κ). Also shown in Fig. 14 are the predictions by Daou et al. [7], which show nearly the same slope as the experimental data but somewhat larger κ at extinction. (This in turn means that the “heat-loss extinction” curve in Fig. 1 should be shifted slightly to the right but does not significantly affect the choice of $d = 0.75$ as the baseline condition.)

Finally, we compare the relationship between U_{edge}/S_L and $(\rho_u/\rho_b)^{1/2}$ to the predictions by Ruetsch et al. [9], who considered the effects of thermal expansion on adiabatic triple-flame propagation in unstrained two-dimensional mixing layers in the

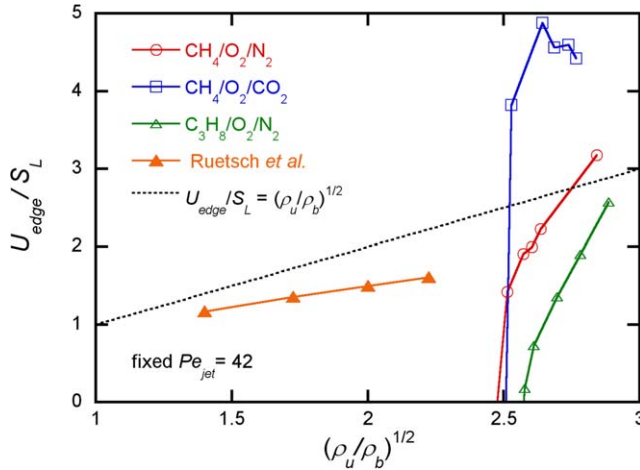


Fig. 15. Comparison of measured values of U_{edge}/S_L as a function of density ratio for $Pe_{\text{jet}} = 42$ and comparison to theoretical predictions by Ruetsch et al. [9].

limit of small mixture fraction gradient (corresponding to small σ). Of course, flow and transport are different in the unstrained mixing layer compared to the plane-strain counterflow employed here, but nevertheless it is instructive to see how well the same thermal expansion effects apply. The comparison is shown in Fig. 15. For the experimental data, the value of U_{edge}/S_L is taken at the σ corresponding to $Pe_{\text{jet}} = 42$ because this provides the highest value of U_{edge}/S_L for $Le \geq 1$ (see Figs. 7a and 12) and thus is the condition least influenced by heat losses (at lower σ) or strain-induced weakening of the flame (at higher σ). For $Le < 1$, $Pe_{\text{jet}} = 42$ does not provide the highest value of U_{edge}/S_L because in this case moderate strain strengthens the flame. Nevertheless, for $Le < 1$ the value of U_{edge}/S_L shown in Fig. 15 is still taken at the σ corresponding to $Pe_{\text{jet}} = 42$ because at this low σ , U_{edge}/S_L is least influenced by either heat loss or strain effects. It should be noted that it is not possible to obtain a large range of ρ_u/ρ_b experimentally because this would require a large range of T_f ; for high activation energy systems such as hydrocarbon–oxygen flames this means that only a narrow range of mixtures has values of T_f that are neither too low (so that total extinction occurs, corresponding to $\rho_u/\rho_b < 2.5$ in Fig. 15) or too high (and thus have impractically high S_L). Fig. 15 shows that for all mixtures, there are no data below $\rho_u/\rho_b \approx 2.5$, which corresponds to the weakest mixture sustaining any combustion, which has the lowest attainable T_f (≈ 1800 K) and thus highest ρ_b . Just above this critical value of ρ_u/ρ_b , the maximum values of U_{edge} are negative (not shown) but rise quickly to positive values for slightly larger ρ_u/ρ_b . The $Le \approx 1$ mixtures ($\text{CH}_4/\text{O}_2/\text{N}_2$) rise to values of U_{edge}/S_L that are close to extrapolated predictions of Ruetsch et

al. [9], whereas the $Le < 1$ mixtures ($\text{CH}_4/\text{O}_2/\text{CO}_2$) are significantly higher and $Le > 1$ ($\text{C}_3\text{H}_8/\text{O}_2/\text{N}_2$) mixtures are significantly lower. One could extrapolate the trends shown in Fig. 15 to speculate that if much higher values of ρ_u/ρ_b were achievable (corresponding to much higher values of Pe_{flame}) the data for all three Le would converge to similar values of scaled U_{edge} that are close to Ruetsch et al.'s predictions. Consequently, while thermal expansion effects described by Ruetsch et al. are certainly an important factor for assessing edge-flame propagation speeds in slot-jet counterflows, the effects of heat loss and Lewis number make it impractical to base estimates of U_{edge} solely on thermal expansion effects.

5. Conclusions

The propagation rates of advancing and retreating nonpremixed edge flames in a slot-jet counterflow were measured as a function strain rate for varying jet spacing, mixture strength, stoichiometric mixture fractions, and Lewis numbers. For a given mixture family, edge-flame propagation rates for different mixture strengths scaled by a thermal expansion factor and the laminar burning velocity of a stoichiometric premixture of the reactant streams correlated well with a nondimensional flame thickness ε related to the strain rate and laminar burning velocity. For mixtures families with lower/higher reactant Lewis numbers, the edge-flame speeds were much higher/lower. Also, edge-flame speeds were higher/lower for higher/lower stoichiometric mixture fractions. Two extinction limits were identified, one at low strain due to heat loss to the jets and one at high strain due to insufficient residence time for chemical

reaction. The low-strain limit could be characterized solely in terms of a dimensionless heat-loss parameter κ and was practically independent of all other experimental factors. The high-strain limit is strongly influenced by the reactant Lewis numbers and stoichiometric mixture fraction, but is independent of κ and thus mixture strength for a given mixture family. For some mixtures, “triple flames” or “short-length edge flames” were observed, but only for very narrow ranges of conditions near the low-strain extinction limits. These results are mostly consistent with theoretical predictions, except for the flame structures and propagation rates near the low-strain extinction limits. This is proposed to be due to the differences between the theoretical assumption of volumetric heat losses and the experimental situation of gradient-driven heat losses to the jet exits.

Acknowledgments

M.S.C. was supported by the Korea Research Foundation (KRF) Grant (M01-2004-000-10055-0). The authors are grateful to J.-B. Liu, O.C. Kwon, and M.K. Kim for their valuable assistance with the experiments.

References

- [1] J.D. Buckmaster, *Prog. Energy Combust. Sci.* 28 (2002) 435–475.
- [2] T.G. Vedarajan, J.D. Buckmaster, *Combust. Flame* 114 (1998) 267–273.
- [3] T.G. Vedarajan, J.D. Buckmaster, P.D. Ronney, *Proc. Combust. Inst.* 27 (1998) 537–544.
- [4] J. Daou, A. Liñán, *Combust. Flame* 118 (1999) 479–488.
- [5] J.D. Buckmaster, *Combust. Sci. Technol.* 115 (1996) 41–68.
- [6] J. Daou, A. Liñán, *Combust. Theory Modelling* 2 (1998) 449–477.
- [7] R. Daou, J. Daou, J. Dold, *Proc. Combust. Inst.* 29 (2002) 1559–1564.
- [8] R. Daou, J. Daou, J. Dold, *Combust. Theory Modelling* 8 (2004) 683–699.
- [9] G.R. Ruetsch, L. Vervisch, A. Liñán, *Phys. Fluids* 7 (1995) 1447–1454.
- [10] Y.S. Ko, T.M. Chung, S.H. Chung, *KSME Int. J.* 16 (2002) 1710–1718.
- [11] G. Amantini, J.H. Frank, A. Gomez, *Proc. Combust. Inst.* 30 (2004) 313–321.
- [12] W.F. Carnell, M.W. Renfro, *Combust. Flame* 141 (2005) 350–359.
- [13] W.T. Ashurst, A.R. Kerstein, R.M. Kerr, C.H. Gibson, *Phys. Fluids* 30 (1987) 2343–2353.
- [14] C.J. Rutland, A. Trouvé, *Combust. Flame* 94 (1993) 41–57.
- [15] G.P. Smith, D.M. Golden, M. Frenklach, N.W. Moriyarty, B. Eiteneer, M. Goldenberg, C.T. Bowman, R.K. Hanson, S. Song, W.C. Gardiner Jr., V.V. Lissianski, Z. Qin, http://www.me.berkeley.edu/gri_mech/.
- [16] Z. Qin, V.V. Lissianski, H. Yang, S.W.C. Gardiner, S.G. Davis, H. Wang, *Proc. Combust. Inst.* 28 (2000) 1663–1669.
- [17] D. Bradley, *Proc. Combust. Inst.* 24 (1992) 247–262.
- [18] C.M. Vagelopoulos, F.N. Egolfopoulos, C.K. Law, *Proc. Combust. Inst.* 25 (1994) 1341–1347.
- [19] M.L. Shay, P.D. Ronney, *Combust. Flame* 112 (1998) 171–180.
- [20] A. Kitajima, H. Torikai, M. Takeuchi, M. Oya, *Combust. Flame* 137 (2004) 93–108.
- [21] D.B. Spalding, *Proc. R. Soc. London A* 240 (1957) 83–100.
- [22] R. Chen, R.L. Axelbaum, *Combust. Flame* 142 (2005) 62–71.